Geomechanics and Engineering, *Vol. 35, No. 3 (2023) 271-286*
https://doi.org/10.12989/gae.2023.35.3.271

Uplift capacity and failure mechanism for belled pile embedded in soft-rock ground

Gyeong-o Kang[1a], Young-sang Kim[2b], Jaehong Kim[3c] and Jung-goo Kang[*1,]

[1]*Department of Civil Engineering, Gwangju University, 277 Hyodeck-ro, Nam-gu, Gwangju, 61743, Republic of Korea*
[2]*Department of Civil Engineering, Chonnam National University, 77 Yongbong-ro, Buk-gu, Gwangju 61186, Republic of Korea*
[3]*Department of Civil Engineering, Dongshin University, 67 Dongsindae-gil, Naju-si, Jeollanam-do, 58245, Republic of Korea*

(*Received July 11, 2023, Revised October 5, 2023, Accepted October 10, 2023*)

Abstract. This study aims to investigate the failure mechanism and uplift capacity of a belled pile embedded in soft rock. The laboratory model test for evaluating the uplift capacity of a belled pile at the circular chamber was conducted for two belled angles (0° and 12°) and penetration depths (160 mm and 80 mm) under the same strength condition on soft-rock ground. In addition, to investigate the failure mechanism of the belled pile, the failure behavior of the belled pile embedded in soft-rock ground was analyzed under different conditions of the belled angle (12° and 30°) and strength at the soft-rock ground (0.3 MPa and 1 MPa) via image analysis in a half-circular chamber. A higher belled angle and ground strength resulted in a higher uplift capacity under the same penetration depth. In addition, the uplift capacity under the same belled angle and ground strength increased with penetration depth. For the image analysis, the shape of the failure surface was an inverted cone regardless of the test conditions. In addition, the failure mechanism was observed in three stages: (a) static, (b) compression, and (c) formation of the failure surface. A new predictive model for the uplift capacity of the belled pile applicable to the soft-rock ground was proposed based on the result. In addition, the predicted value was in good agreement with the measured value. Therefore, this model can be very useful for estimating the uplift capacity of a belled pile embedded in soft-rock ground.

Keywords: belled pile; failure mechanism; predictive model; soft-rock; uplift capacity

1. Introduction

Horizontal loads generated during natural disasters, such as typhoons, earthquakes, and tsunamis can cause the collapse of structures. Belled piles are effective and economical solutions for improving the uplift capacity of structures owing to the shape of the extended pile tip (Moayedi and Mosallanezhad 2017). This feature means that the belled pile can effectively cope with the horizontal load applied to the structure. Therefore, these piles have been used in the foundations for various civil structures (e.g., high chimneys, power transmission towers, and coastal structures) subjected to large horizontal loads.

Nowadays, belled piles can even be constructed on soft-rock ground with an N value of more than 50 due to developments in construction technology (Qian *et al.* 2015, Yang *et al.* 2018, Wang *et al.* 2020, Hu *et al.* 2023). The belled pile has been expanded to the foundation construction methods for various structures, such as apartments and mansions as well as civil structures (Yamazaki 1995, Maeno *et al.* 1997, Moayedi and Mosallanezhad 2017). However, their usability is limited because the precise mechanisms of different types of ground have not been identified. Hence, the evaluation and construction of most belled piles applied to soft rock ground are based on field experiment results.

Most previous studies have investigated the uplift capacity of conventional piles, anchor plates, helical piles, and screw piles (Spagnoli *et al*. 2015, Emirler *et al.* 2016, Mohajerani *et al*. 2016, Basha and Azzam 2018, Ukritchon and Keawsawasvong 2019, Roy *et al.* 2021, Spagnoli and de Hollanda Cavalcanti Tsuha 2020, Santos Filho and Tsuha 2020, Sharif *et al.* 2021, Vashishtha *et al.* 2021, Prakash and Muthukkumaran 2021, Perumalsamy and Ranganathan 2022). Several predictive models for the uplift capacity of piles have been proposed based on the laboratory model test, field test, and numerical analysis (Majer 1955, Balla 1961, Robinsky and Morrison 1964, Downs and Chieurzzi 1966, Matsuo 1967, Matsuo 1968, Meyerhof and Adams 1968, Das 1983, Murray and Geddes 1987, Chaly *et al*. 1991, Dash and Pise 2003, Mohajerani *et al*. 2016, Aksoy *et al.* 2016, Mohajerani *et al.* 2016, Mosallanezhad and Moayedi 2017, Cerfontaine *et al.* 2019, Sakr *et al.* 2020, Lin *et al.* 2022, Cheng *et al.* 2022, Vignesh and Muthukumar 2023). However, only a few studies on the belled pile exist, and most studies on conventional piles and anchor plates have been conducted on clayey and sandy grounds (Matsuo 1967, Matsuo 1968, Ilamparuthi and Muthukrishnaiah 1999, Ilamparuthi and Dickin 2001,

∗Corresponding author, Ph.D.
E-mail: cocoya0305@gmail.ac.kr
[a]Assistant Professor
E-mail: gokang@gwangju.ac.kr
[b]Professor
E-mail: geoyskim@jnu.ac.kr
[c]Assosiate Professor
E-mail: woghd@dsu.ac.kr

ISSN: 2005-307X (Print), 2092-6219 (Online)

Ilamparuthi *et al.* 2002, Rao *et al.* 2006, Merifield 2011, Tsuha *et al*. 2012, Leshchinsky *et al.* 2012, Faizi *et al.* 2015, Moayedi and Mosallanezhad 2017, Kranthikumar *et al.* 2017, Ukritchon and Keawsawasvong 2019, Ali and Abbas 2019). Previously, belled piles were used in transmission line towers and designed to improve the uplift capacity of the foundation due to large horizontal loads imposed by the wind. Belled piles and enlarged piers have been studied by some researchers (Kishida 1963, Dickin and Leung 1990, Chae *et al*. 2012, Chae *et al*. 2012, Honda 2015, Lin *et al.* 2015, Hirai *et al.* 2016, Yang *et al.* 2018, Wang *et al.* 2020).

Dickin and Leung (1990) conducted a centrifuge model test to investigate the uplift behavior of an enlarged pile on sandy ground. In addition, they compared this to an existing uplift-capacity model of an anchor plate to verify the obtained results. Many previous theories on anchor plates overestimate the uplift capacity for belled piles in both dense and loose sandy ground. The proposed empirical equation, derived from the anchor plate equation in dense sand, yielded reasonable values. Hirai *et al*. (2016) performed field experiments on in-situ concrete piles with one or two enlarged parts of bases to evaluate the uplift capacity behavior of belled piles. The belled pile exhibited a higher uplift capacity with reference to the surrounding ground than the conventional pile. Honda *et al.* (2011) conducted field experiments, centrifugal model tests, and two-dimensional discrete element (DE) analysis to evaluate the uplift capacity of belled and multi-belled piles in dense sand. They proposed a continuity equation for predicting the uplift capacity that satisfies the relationship between the displacement vector and the volume change of the ground.

The uplift capacity of belled piles on soft rock was recently studied (Chae *et al.* 2012, Yang *et al.* 2018, Wang *et al*. 2020, Hu *et al*. 2023). Most research has focused on field tests and suggesting methods for evaluating uplift capacity using experimental results and finite element method (FEM) analysis. Cho and Na (2012) conducted field experiments on the uplift capacity of belled piles at four locations in Abu Dhabi, United Arab Emirates to consider the horizontal load and uplift capacity of coastal structures in sandstone ground. They proposed a semi-empirical method to calculate the ultimate uplift capacity of sandstone ground through field tests and 3D finite element method (FEM) analysis. Yang *et al*. (2018) investigated the uplift behavior of short piles using a rock-socket belled pile via field tests. The results confirmed that the pull-out resistance could be improved, ranging from 54.9% to 34.7%, depending on the pile bell shape. Wang *et al.* (2020) performed field tests for five cases involving ground with an upper clay layer and a lower thick sandstone layer to design a transmission tower foundation. They suggested that the ultimate uplift capacity can be predicted using a hyperbolic model, a load–displacement curve, and a reduction parameter. Despite several studies, designing the uplift capacity of belled piles for soft rock remains very limited. Currently, although the belled pile is buried in soft rock, the evaluation and design of belled piles has been based on data on sandy and clayey grounds. In addition, because most studies on soft rock involved field tests and FEM analysis, elucidating the failure and uplift behavior of a belled pile embedded in soft rock ground has been difficult. In addition, the failure and uplift behavior of belled piles installed in soft rock ground may become a basis for critical design variables and optimal design criteria according to various ground conditions. Therefore, the investigation of failure mechanism and failure shape was required to clearly evaluate the uplift capacity of belled piles embedded in soft rock ground.

This study aims to investigate the failure mechanism and uplift capacity of the belled pile embedded in soft-rock ground. The laboratory model test for evaluating the uplift capacity of a belled pile at the circular chamber conducted for different belled angles (0° and 12°) and penetration depths (160 mm and 80 mm) under the same strength condition in soft-rock ground. In addition, to investigate the failure mechanism of a belled pile, the failure behavior of a belled pile embedded in soft-rock ground was analyzed by varying the belled angle (12° and 30°) and strength at the soft-rock ground (0.3 MPa and 1 MPa) by performing image analysis in a half-circular chamber. A new predictive model for the uplift capacity of a belled pile applicable to soft-rock ground was then proposed based on the result.

2. Experimental method

2.1 Test condition

Table 1 lists the test conditions of the laboratory model test. Laboratory model experiments were conducted for three cases in circular and half-circular model chambers. The circular model test was performed under stress-controlled conditions by varying the penetration depth (80 mm and 160 mm) of conventional and belled piles with a 12° belled angle. The half-circular model test was performed using two types of belled piles (12° and 30°) in soft-rock ground with different strengths (0.3 MPa and 1 MPa) under a strain-controlled condition. The soft-rock ground condition in the half-circular model test was achieved by dividing the soft-rock of the lower layer and the sand of the upper layer to consider the field construction condition. The experiment was observed using monitoring equipment installed on the front of the half-circular model chamber.

2.2 Laboratory model test apparatus

Fig. 1 shows the laboratory model test apparatus. The parts of the model test device are a loading system, measuring device, model piles, and model chambers. The loading system consists of Bellofram (BF) cylinder (air cylinder) and a screw jack. The BF cylinder and screw jack were used to control the uplift load in the belled pile (Fig. 1(a)). Notably, the BF cylinder and screw jack were used for stress and strain-controlled in the laboratory model tests, respectively. Here, the stress-controlled operation method involves applying load to the belled pile without considering the displacement. The stress-controlled method was utilized to measure the uplift capacity of a belled pile at

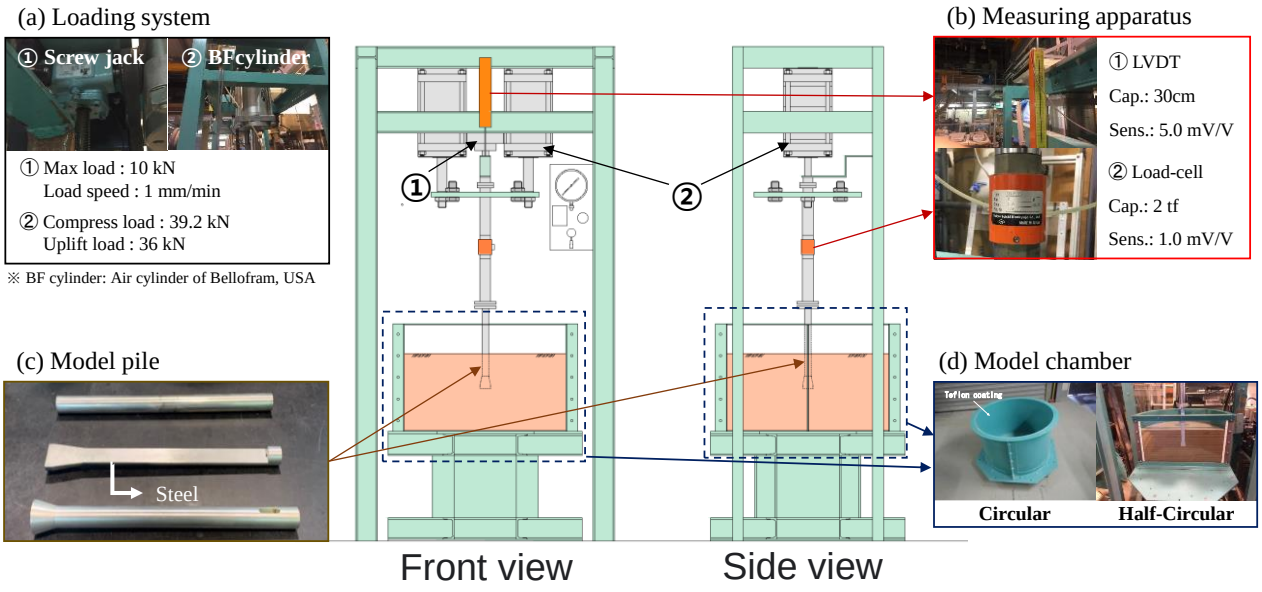

Fig. 1 Laboratory model test apparatus: (a) loading system, (b) measuring device, (c) model pile, and (d) model chamber

Table 1 Test conditions of the laboratory model test

Test ID	Chamber type	Loading type	Belled angle (θ_i)	Penetration depth (mm)		Ground strength
			(°)	Soil-cement	Sand	(MPa)
P00L16-1	Circular	Stress	0	160	-	1
P12L16-1			12	160	-	1
P12L08-1			12	80	-	1
HP12L88-1	Half-circular	Strain	12	80	84	1
HP12L88-0.3			12	80	82	0.3
HP30L88-1			30	80	84	1

the circular chamber. In addition, two BF cylinders were installed at the top of the laboratory model test system, and the maximum uplift load capacity at each cylinder was about 20 kN. The compression and uplift loads were constantly increased to an air pressure of 0.6 MPa, and their maximum values were approximately 35 kN and 33 kN, respectively. In contrast, the screw jack was employed in the strain-controlled test to monitor the failure surface of the belled pile with the evaluation of the uplift capacity at the half-circular chamber without a variation in air pressure. The maximum load capacity of the screw jack was measured using a load cell to be 10 kN. Table 2 lists the loading speed of uplift and compression according to the scale level. The error occurred in the 2nd decimal place of the loading speed, which is considered reliable. This experiment was performed at an uplift speed of approximately 1 mm/min.

The measuring devices in the laboratory model test were the linear variable displacement transducer (LVDT) and load cell (Fig. 1(b)). The LVDT can measure up to 50 cm. The two devices were connected to the data logger, and data were collected 200 times per minute to ensure test accuracy. A load cell with a maximum capacity of 2 t was used to minimize noise during uplift loading.

The circular pile and half-circular pile were employed in laboratory model tests depending on the purpose of test. The circular pile was used to investigate the uplift capacity of the belled and conventional pile in the laboratory model test. The diameter of the belled and conventional pile tip were 30 mm and 48 mm, respectively: the belled angles of the belled pile was 12°. The total length of all circular piles was 370 mm, but the length of the straight part of the belled pile depended on the belled angle: 313 mm for the 12° belled angle. The half-circular belled pile was used to monitor the failure surface between the pile and ground and to evaluate the uplift capacity of the belled pile. The diameter of the belled pile was 24 mm, and the belled angles were 12° and 30°. In addition, the total length of the piles was 360 mm, but the lengths of the straight part of the belled pile were 283 mm and 314 mm with 12° and 30° belled angles. An additional half-circular belled pile shaft 30 mm in diameter and 20 mm in length served as a connecting part during the pile uplift test (Fig. 1(c)).

The model circular and half-circular chambers were used for the corresponding model tests. The circular chamber was used to measure the uplift capacity of the model pile, whereas the half-circular chamber was used to monitor the failure surface between the pile and soft-rock

Table 2 Loading speed of uplift and compression according to the scale level

Step	Scale	Compression speed (mm/min)		Uplift speed (mm/min)	
L01	2	3.86	3.84	-3.85	-3.87
L02	2.7	5.45	5.44	-5.48	-5.46
L03	3	6.44	6.45	-6.51	-6.52
L04	4	9.06	9.08	-9.08	-9.09

Table 3 Strength standards according to rock type (JGS: 3811-2004)

Type	Extremely hard-rock	Hard-rock	Medium-rock	Swelling hard-rock
UCS* (kgf/cm2)	1000 or more	500~1000	100~599	100~500
Type	Anisotropic medium-rock	Sandy soft-rock	Clayey soft-rock	Swelling hard-rock
UCS (kgf/cm2)	100~500 Anisotropic rock (Gneiss etc.)	10~100 Soft sand (weathered rock)	10~100 Clayey rock	10~100 Bentonite

*UCS: Uniaxial compressive strength

Table 4 Physical properties of the Kumamoto silica sand (K7) and chemical properties of quick-hardening cement

Kumamoto silica sand (K7)		Quick-hardening cement (JIS R 5210)	
Physical properties	Value	Chemical properties	(%)
Liquid limit, LL (%)	N. P	SiO2 (%)	20.4 ~ 21.59
Plastic limit, PL (%)	N. P	Al2O3 (%)	4.56 ~ 5.48
Specific gravity, Gs	2.63	Fe2O3 (%)	2.58 ~ 2.88
Fine-grained soil (%)	15.60	CaO (%)	65.12 ~ 66.05
Unified Soil Classification System	SM	MgO (%)	0.93 ~ 2.03
Maximum density,ρmax (g/cm3)	1.57	SO3 (%)	1.68 ~ 2.51
Minimum density,ρmin (g/cm3)	1.20	ig. Loss (%)	0.62 ~ 2.13
Internal friction angle (°)	42 (Dr = 80%)	insol. (%)	0.20 ~ 1.00

ground to evaluate the uplift capacity of the belled pile. These chambers were made of low-deformation steel. Regarding the half-circular chamber, the observation window was constructed using an acrylic plate 10 mm thick for monitoring the failure surface (Fig. 1(d)). The diameter and height of the model chambers were 500 mm and 750 mm, respectively. To negate the impact area of the load, the diameter of the model chamber was set to 10 times that of the pile. Kishida (1963) reported that a ratio of the chamber diameter to pile diameter ranging from 3 to 8 can negate the impact area of the load. In addition, the inside of all chambers was coated with Teflon to minimize wall friction.

Fig. 2 shows the image analysis result obtained through the preliminary experiment. In this study, image analysis was performed by extracting the image corresponding to an uplift displacement of 1 mm from the monitored image. Accordingly, the shape of the failure surface was clearer than that of colored sand. A 4k video camera was used to monitor the experimental progress in the half-circular chamber. It was installed in front of the half-circular chamber and recorded the entire experiment. The images of the area between the pile and ground were captured for a displacement of up to 20 mm. Image analysis of the captured image was performed by changing the color before and after the deformation to confirm the shape of the failure surface between the pile and ground.

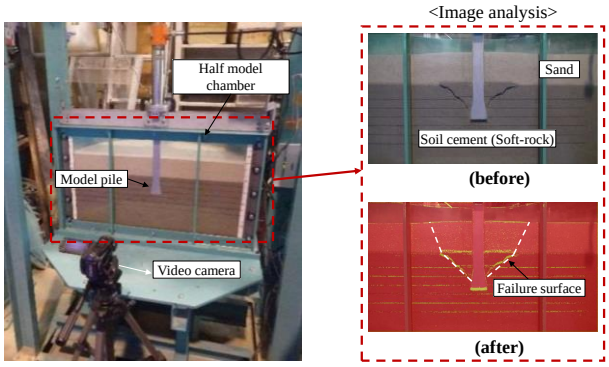

Fig. 2 Image analysis in the monitoring system

2.3 Laboratory model test apparatus

Table 3 lists the strength standards according to rock type (JGS: 3811-2004). In this study, the soft-rock strength for rocky ground construction was selected to prepare the model ground in the laboratory model experiment. Soft rock can typically be divided according to strength as weathered rock and clayey soft-rock, and its strength ranges from 10 to 100 MPa. The laboratory model tests in this study were performed at a 1/50 scale of the 50 MPa of field condition.

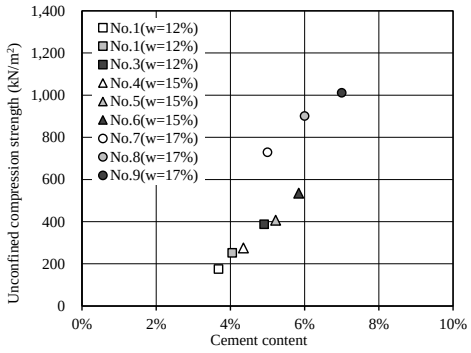

Fig. 3 The result of trial mixing test for the unconfined compression strength of soft-rock model ground

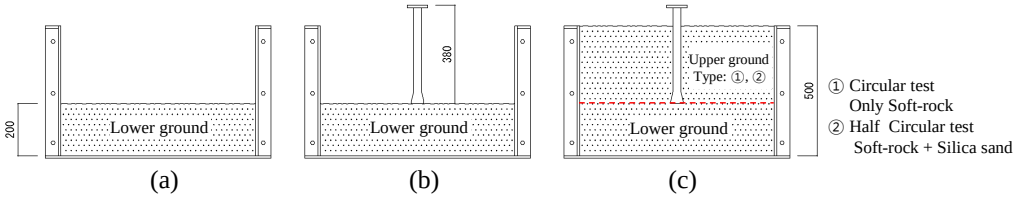

Fig. 4 The preparation process of soft-rock model ground: (a) preparation of lower ground, (b) pile installation, and (c) preparation of upper ground

Therefore, the strength of the model ground was set to approximately 1 MPa. For the half-circular model test, 0.3 MPa soft-rock ground was used to account for the effect of ground strength.

Table 4 presents the physical properties of the materials used in the model ground. To simulate the soft rock on the model ground, Kumamoto silica sand (K7), quick-hardening cement (JIS, 2009), and water were used as the basic materials. K7 is silty sand with a specific gravity of 2.63; fine content of 15.6%; and maximum and minimum densities of 1.57 and 1.20, respectively. The 7 d curing strength of quick-hardening cement is approximately 85% that of the 28 d curing strength of ordinary Portland cement.

The trial mixing test was performed at various cement and water contents to determine the rock ground strength. Nine cases of trial mixing were considered according to the mixing ratio (water content: 12%, 15%, 16%, and 17% and cement content: 4%, 5%, 6%, and 7%). The curing period of the trial mixing test was set as 7 d because quick-hardening cement was used in this study.

Fig. 3 shows the results of the trial mixing test. Notably, 1 MPa corresponding to the soft-rock ground in this study was confirmed at a K7 mixing ratio content of 76%, quick-hardening cement content of 7%, and water content of 17%. For a comparative study, a strength of 0.3 MPa in soft-rock ground was additionally set for a K7 mixing ratio content of 80%, quick-hardening cement content of 4%, and water content of 16%.

In the circular model test, the piles were penetrated at 80 mm (belled pile) and 160 mm (conventional and belled piles) under 1 MPa soft-rock ground to examine the effect on pile shape and penetration depth. For the half-circular model test, the pile penetration depth was set to 80 mm, and the upper sand layer was 80 mm thick with a relative density of 80% for K7.

Fig. 4 shows the method of preparing the soft-rock model ground. The model ground was prepared in three stages: 1) preparation of the lower ground, 2) installation of the pile, and 3) preparation of the upper ground (soft-rock ground in the circular model test and sand ground in thehalf-circular model test). In all experiments, the lower ground thickness was 200 mm, and its strength was set to equal to the strength of the upper ground to observe the ground behavior at the lower part of the pile. After curing, the model pile was placed on the lower ground and fixed to the uplift connection part. The upper soft-rock ground during the circular model test was equal to the penetration depth of each experiment, and the upper grounds of the half-circular model test were prepared as two layers, namely 8 cm of soft-rock ground and 8 cm of sand ground from the pile tip.

Air bubbles and gaps in the soft-rock ground were minimized through compaction, and the mixture was poured after calculating the volume corresponding to the 5 cm height in the chamber. This method was repeated up to the set height to form the soft-rock ground. The method of composing the soft-rock ground in the half-circular model test was equal to that in the circular model test. In addition, the sand layer was formed through compaction after calculating the sand weight corresponding to a relative density of 85%; this was then poured on the cured soft-rock ground.

3. Results and discussion

3.1 Uplift capacity of pile in the circular chamber test

Fig. 5 shows the model test results in the circular chamber according to the penetration depth and pile type (conventional and belled piles). The stress-controlled

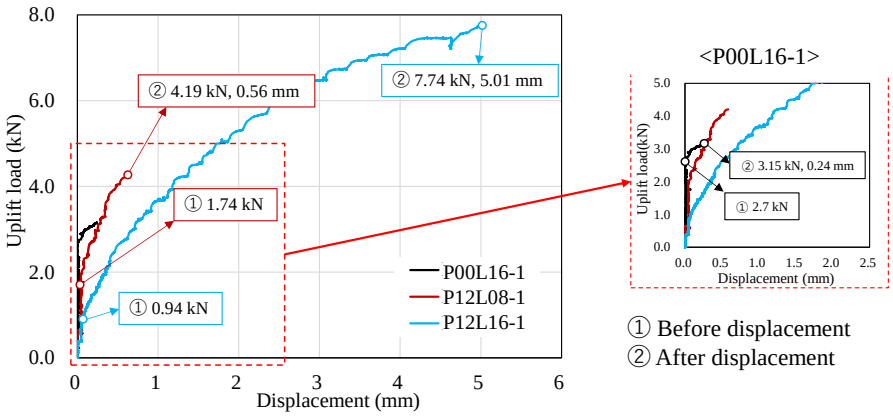

Fig. 5 Uplift load with the vertical displacement according to the penetration depth and pile type (conventional pile belled pile) in the circular chamber test

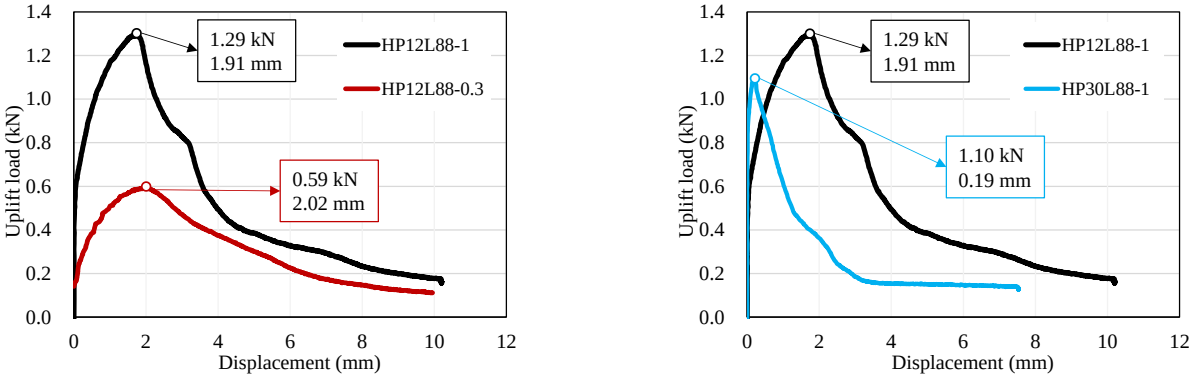

Fig. 6 Uplift load with the vertical displacement according to ground strength (0.3 MPa and 1 MPa) and belled angle (12° and 30°): (a) Comparison of ground strength and (b) Comparison of belled angle

operation is a method of measuring the bearing capacity and uplift capacity of piles in the field. Therefore, in a circular model chamber, the stress-controlled method was adopted to measure the uplift capacity of belled piles. In the stress-controlled method, the section where no deformation occurs despite the increase in stress, that is, the uplift load, refers to the uplift capacity that the belled pile can resist without deformation in the soft-rock ground. In addition, the maximum uplift load in the stress-controlled method means the section where stress does not increase despite the deformation of the ground, that is, failure occurs. Therefore, the experiment terminates immediately after the maximum uplift load is reached. The uplift capacity of the conventional pile at a 16 cm penetration depth (P00L16-1) increased to 2.7 kN without vertical displacement, and the maximum uplift capacity required for shear failure was 3.15 kN at a vertical displacement of 0.24 mm. On the other hand, the uplift capacity of the belled pile with a belled angle of 12° and 16 cm penetration depth (P12L16-1) continuously increased from 0.94 kN, and the maximum uplift capacity was 7.74 kN at a 5.01 mm vertical displacement. Moreover, for the belled pile with a belled angle of 12° and penetration depth (P12L08-1) of 8 cm, the uplift capacity without the vertical displacement was 1.74 kN and maximum uplift capacity was 4.19 kN with a 0.56 mm vertical displacement.

The uplift capacity test revealed that for the same penetration depth (16 cm), the maximum uplift capacity of the belled pile was approximately 2.8 times higher than that of the conventional pile. Regarding the belled pile at 8 cm penetration depth and conventional pile at 16 cm penetration, the maximum uplift capacity of the belled pile was approximately 1.33 times higher than that of the conventional pile, even though the belled pile had half the penetration depth of the conventional pile. Accordingly, the belled pile has a more desirable uplift resistance than the conventional pile.

The belled piles at different penetrations (8 cm and 16 cm) exhibited a continuous increase in displacement and uplift capacity from the beginning of loading, whereas the conventional pile displacement did not exhibit this phenomenon until 85% (2.7 kN) of the maximum uplift capacity at ground failure. At the maximum uplift load, the total displacement of the conventional pile was 0.24 mm, which was much smaller than that of the belled pile at the maximum uplift load. This is attributable to the maximum uplift load being generated at a relatively small displacement because the uplift resistance of the conventional pile only depends on the circumferential friction. However, a belled pile induces compression (displacement) in the surrounding ground from the tip of the pile when pulled out due to its shape. Accordingly, the

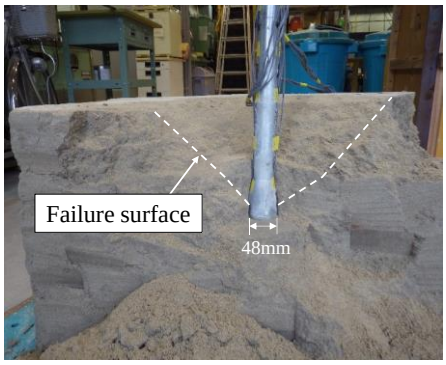

Fig. 7 The failure shape of the soft-rock ground after terminating the pull-out test of belled pile

compression of the surrounding ground increases not only the uplift load but also the displacement.

3.2 Uplift capacity of pile in the half-circular chamber test

Fig. 6 shows the results of the uplift capacity in the half-circular test according to the strength (0.3 MPa and 1 MPa) of the soft-rock ground and belled angle (12° and 30°). As mentioned earlier, the penetration depth of the pile into the soft-rock ground was 8 cm at the tip of the pile in the half-circular model experiment, and the upper part was homogeneous: 8 cm at a relative density of 85% and comprising Kumamoto silica sand.

Fig. 6(a) shows the results of different soft-rock layer strengths for the same belled angle (12°). The displacement and maximum uplift load for 1 MPa and 0.3 MPa ground strengths (HP12L88-1 and HP12L88-0.3) were 1.29 kN at 1.91 mm and 0.59 kN at 2.02 mm, respectively. The maximum uplift load of the soft-rock ground with a strength of 1 MPa was approximately 2.2 times higher than that of the soft-rock ground with a strength of 0.3 MPa. The difference in the maximum uplift load during the half-circular test performed under the strain loading condition was confirmed to be dependent on the ground strength.

Fig. 6(b) shows the comparison results for two types of belled angles (12° and 30°) at a ground strength of 1 MPa. The maximum uplift load of 1.10 kN was developed for the 30° belled pile at a displacement of 0.19 mm (HP30L88-1). This result demonstrated that the maximum uplift load of the 12° belled pile was approximately 1.17 times greater than that of the 30° belled pile at the same ground strength. In addition, the displacement of the 30° belled pile under maximum uplift load was very small approximately 10% of that of the 12° belled pile. This result suggests that the belled angle of the belled pile under strain loading conditions is an important factor for achieving maximum uplift load and displacement.

3.3 Observation of failure surface and image analysis

After the pull-out test in the circular chamber, the failure shape of the soft-rock ground embedded by the belled pile was observed by the naked eye. For the observation, a portion of the destroyed soft-rock ground was first removed

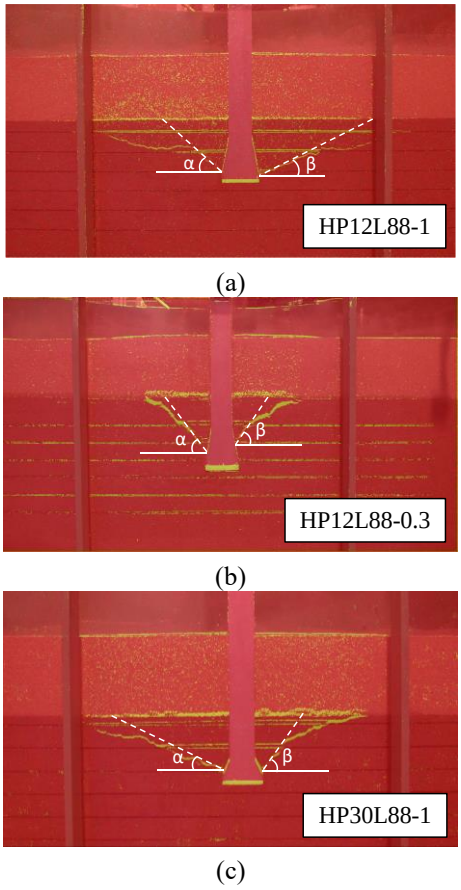

Fig. 8 Failure surface obtained by the image analysis: (a) HP12L88-1, (b) HP12L88-0.3 and (c) HP30L88-1 (α and β: Measured left and right failure angles)

and then the destruction shape could be clearly confirmed. In addition, to quantitatively evaluate the failure surface of the ground, the author additionally performed a half-circular chamber test with the image analysis. Fig. 7 shows the failure shape of the soft-rock ground after terminating the pull-out test of the belled pile in the circular chamber test.

The failure shape of the ground indicates in an inverted cone extending to the ground for both piles regardless of the pile type. However, the failure surface of a belled pile starts at the tip of the pile, whereas that of a conventional pile begins near the ground. Therefore, the uplift resistance of the belled pile produces a wedge effect similar to that of the anchor plates in the ground along with surface friction (Kumar and Kouzer, 2008, 2009, Cerfontaine *et al.* 2019). Therefore, the belled pile has a high resistivity in the ground, beginning at the tip of the pile. Therefore, the shape and size of the failure surface are critical factors in the development of the uplift load of a pile. In addition, the shape and size of the failure surface of the belled pile were overwhelmingly larger than that of the conventional pile under a constant penetration depth. Moreover, the displacement and size of the failure surface according to the maximum uplift load was confirmed in the order of belled pile at a penetration depth of 16 cm, belled pile at a penetration depth of 8 cm, and conventional pile at a penetration depth of 16 cm.

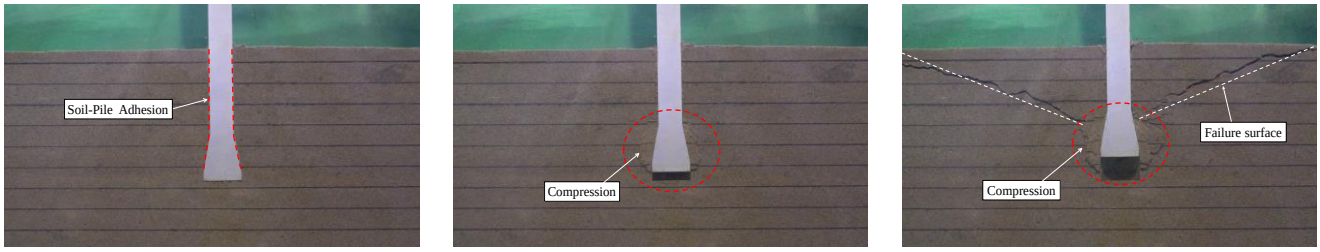

Fig. 9 Formation process of the failure surface of the belled pile in the soft-rock ground: (a) static, (b) compression, and (c) formation of failure surface

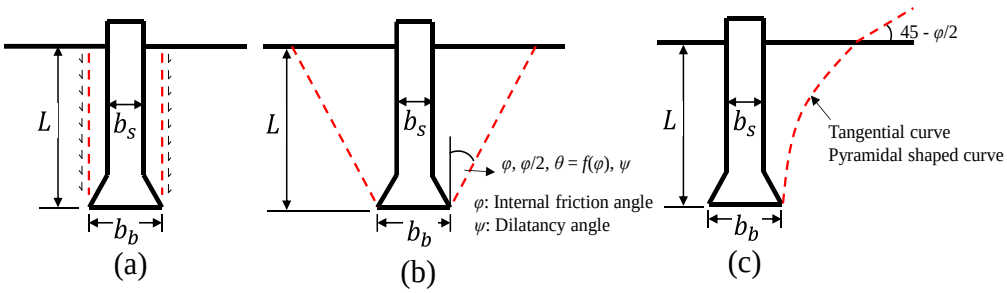

(a) Vertical slip surface model: Majer (1955)
(b) Inverted truncated cone model: Downs and Chieurzzi (1966); Clemence and Veesaert (1977); Murray and Geddes (1987); Sutherland et al. (1982); Vermeer and Sutjiadi (1985)
(c) Curved slip-surface model: Balla (1961); Meyerhof and Adams (1968)

Fig. 10 Existing representative failure surface

To validate the formation of failure surface, the image analysis was carried out under the different belled angle and ground strength. Fig. 8 shows the failure surface obtained by the image analysis. As mentioned above, the failure shape of the lower soft-rock ground also indicates in an inverted cone in all half-circular model tests. However, the shape and size of the failure surface of the belled pile differed depending on the belled angle and ground strength. The size of the failure surface increased in the order of HP12L88-1, HP30L88-1, and HP12L88-0.3, and this result means that the failure surface is formed widely at the low belled angle and the high ground strength.

4. Empirical equation for estimating the uplift capacity

4.1 Failure mechanism of soft-rock ground

An additional model experiment was conducted to monitor the formation of the failure surface during the uplift of a belled pile in soft-rock ground. The experimental conditions were a penetration depth of 16 cm, belled pile of 12°, and soft-rock ground strength of 1 MPa. The pull-out speed was set to 1 mm/min as the strain loading condition.

Fig. 9 shows the formation process of the failure surface of the belled pile in soft-rock ground. Accordingly, the failure surface of the soft-rock ground during the uplift displacement of the belled pile can be divided into three stages: (a) static, (b) compression, and (c) formation of the failure surface.

(a) Static condition: in this state, no uplift displacement is applied, and the uplift resistance of the pile depends on adhesion between the pile and soft-rock ground.
(b) Compression: compression is generated in the ground around the belled part at the tip of the pile under uplift displacement. In this state, the uplift resistance of the belled pile is proportional to the compressive force on the ground surrounding the belled part. During this experiment, compression only occurred in the surrounding ground up to a displacement of 0.5~1 cm, and no failure surface was formed.
(c) Formation of failure surface: after the compression in the ground around the pile was completed, the failure surface formed in the surrounding ground. The expansion of the failure surface starts at the part of the compressed surrounding soil and extends linearly to the ground surface.

According to previous studies, the failure surface of a belled pile on sand and clay grounds is formed simultaneously with the uplift displacement. Further, the shape of the failure surface starts from the tip of the belled pile or the inclined plane of the tip of the belled pile (Majer 1955, Balla 1961, Sutherland 1965, Clemence and Veesaert 1977, Murray and Geddes 1987, Vermeer and Sutjiadi 1985, Meyerhof and Adams 1968). The shape of the failure surface is linear or nonlinear depending on factors such as penetration depth of the pile, relative density of sand, adhesion, internal friction angle, and belled angle. Accordingly, the shape of the existing representative failure surface is shown in Fig. 10.

Table 5 The basic calculation method of conventional pile, belled pile and anchor structures

Pile type	Equation	Parameter	Reference
Conventional pile	$P_{un}=\frac{\pi}{2}K_s b_b \gamma_d L^2 \tan\delta$	P_{un}: net uplift capacity of pile, K_s: lateral earth pressure coefficient, b_b: belled type pile tip diameter, γ_d: dry unit weight, δ: pile - soil friction angle	Das *et al.* (1977)
	$P_{un}=\frac{\pi}{3}L^3 tan^2\frac{\varphi}{2}\gamma_d$	P_{un}: net uplift capacity of pile, φ: internal friction angle, L: penetration depth of pile, γ_d: dry unit weight	Johnson and Kavanagh (1968)
Belled type pile anchor plate	$(P_u)=\gamma_d A_b L^2\left(\frac{L}{b_b}\right)K_u tan\varphi\left[m\left(\frac{L}{b_b}\right)+1\right]+1$	K_u: uplift factor, m: pile tip shape factor, L: penetration depth of pile, A_b: belled type pile tip area, b_b: belled type pile tip diameter, φ: internal friction angle, γ_d: dry unit weight	Meyerhof (1973)
	$(P_u)=\gamma_d A_b L\left(1+2\left(\frac{L}{b_b}\right)tan+\left(\frac{4}{3}\right)\left(\frac{L}{b_b}\right)^2 tan^2\varphi+\left(\frac{b_s}{b_b}\right)^2\right)$	L: penetration depth of pile, b_b:belled type pile tip diameter, b_S: pile column diameter, φ: internal friction angle, γ_d: dry unit weight.	Downs and Chieurzzi (1966)
	$(P_u)=\gamma_d A_b L\left(1+(4.32*tan\varphi-1.58)\left(\frac{L}{b_e}\right)^{1.5}\right)$ $b_e=\sqrt{\frac{\pi {b_b}^2}{4}}$	K_u: uplift factor, m: pile tip shape factor, L: penetration depth of pile, A_b: belled type pile tip area, b_b: belled type pile tip diameter, φ: internal friction angle, γ_d: dry unit weight	Ovesen (1981)
	$(P_u)=\gamma_d A_b L\left\{(F_1+F_3)\left(\frac{4}{\pi}\right)\left(\frac{L}{b_b}\right)^2\right\}$ $F_1+F_3=-0.0171\left(\frac{L}{b_b}\right)^3+0.3057\left(\frac{L}{b_b}\right)^2-1.7937\left(\frac{L}{b_b}\right)+4.0389$	F_1 and F_3 are functions of the peak friction angle which are obtained from the chart. γ_d: dry unit weight, A_b: belled type pile tip area, L: penetration depth of pile, b_b: belled pile tip diameter.	Balla's (1961)

However, the formation of the failure surface in the soft-rock ground differed in two major ways from the failure surface formation in sand and clay grounds. The first is the compression phenomenon of the ground against uplift displacement (Fig. 9(b)), which is caused by the wedge effect between the pile and ground as the belled pile is pulled out (Kumar and Kouzer 2008 and 2009, Cerfontaine *et al.* 2019). The wedge effect of the belled pile exerts a force that pushes it into the surrounding ground via the inclined surface of the tip of the pile. Therefore, the ground around the tip of the pile is compressed to a certain displacement. The second is the shape of the failure surface. As shown in Fig. 9(c), the failure surface for the uplift displacement of the belled pile formed in the soft-rock ground starts at the compression part, unlike the existing failure surface shape. Therefore, the evaluation of the maximum uplift resistance of the soft-rock ground should carefully consider the size and shape of the failure surface.

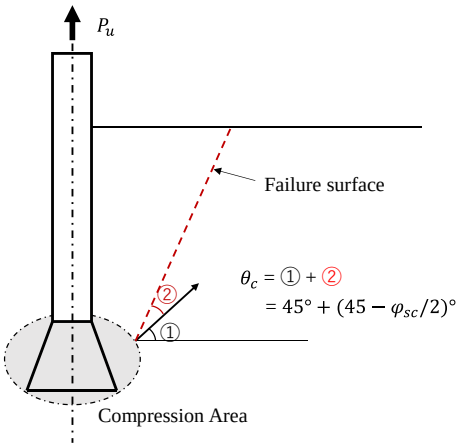

Fig. 11 Assumption of failure surface to propose a predictive model for the uplift capacity

4.2 Prediction of uplift capacity in soft-rock ground

Table 5 lists the previous uplift capacity model of the conventional and belled piles and anchor structures (Das *et al.* 1977, Johnson and Kavanagh 1968, Meyerhof 1973, Downs and Chieurzzi 1966, Ovesen 1981, Balla 1961). The basic uplift resistance calculation method involved defining the sum of the weight of the pile, the weight of soil in the failure surface, and the shear force of the failure surface

after determining the failure surface formed in the ground during pull-out (Eq. (1)). The forementioned research was conducted on cohesive soil and sandy soil, and representative failure surfaces were proposed according to ground conditions.

$$P_u = W_{soil} + W_{pile} + T \quad (1)$$

where the net uplift capacity in Eq. (1) can be expressed as Eq. (2) by excluding the weight of the pile.

$$P_{u(net)} = W_{soil} + W_{pile} \quad (2)$$

Noticeably, the failure surface in the soft-rock ground exhibited a unique feature: it began with the formation of compression in the ground around the pile tip. In addition, according to the model test results, the maximum uplift displacement occurred at a small belled angle. This tendency means that the lower the belled angle, the higher the compression in the surrounding ground. However, this complex failure surface has a limitation when directly applying the predictive model for the uplift capacity. Therefore, three conditions of the failure surface in the soft-rock ground were assumed as follows (Fig. 11):

1. The failure surface starts at the center of the inclined area of the belled pile.
2. The failure surface extends linearly to the ground surface.
3. The angle of failure surface according to the uplift capacity and displacement occurs at the tip compression part, and because the shape of the compression part is not constant, the direction of action of the earth pressure generated in the compression part of the pile tip is assumed to be 45°. Meanwhile, the effects of the uplift capacity and displacement on the behavior characteristics of the belled pile are similar to those in the passive state.

In this study, the predictive model for the uplift capacity of soft-rock ground considers the internal friction angle and shear force in the failure surface as the main parameters. Therefore, to calculate the failure angle and shear force of the failure surface, which are important parameters affecting the size and shape of the failure surface, an additional specimen of the model ground was fabricated,

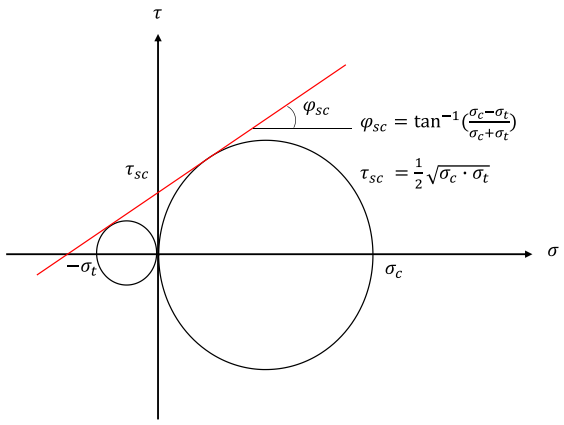

Fig. 12 Coulomb's theory to determine the internal friction angle (φ_{sc}) and shear stress (τ_{sc})

Table 6 Internal friction angle (φ_{sc}), and shear stress (τ_{sc}) of model ground by mixing ratio

Model design strength	Compressive stress σ_c	Tensile stress σ_t	Internal friction angle φ_{sc}	Shear stress τ_{sc}
(MPa)	(kN/m²)	(kN/m²)	(°)	(kN/m²)
1.0	795.6	69.4	60.0	105
	757.9	44.4		
	809.6	55.9		
0.3	261.6	31.5	55	46
	298.1	30.0		
	297.5	23.7		

and the internal friction angle and shear force were calculated by applying Coulomb's failure theory as Eqs. (3) and (4) in Fig. 12 and its result showed in Table 6.

$$\varphi_{sc} = \tan^{-1}\left(\frac{\sigma_c - \sigma_t}{\sigma_c + \sigma_t}\right) \quad (3)$$

$$\tau_{sc} = \frac{1}{2}\sqrt{\sigma_c \cdot \sigma_t} \quad (4)$$

In this study, the internal friction angle calculated via Coulomb's failure theory were assumed to be the failure angle within the failure surface as Eq. (5).

$$\theta = 45° + \left(45 - \frac{\varphi_{sc}}{2}\right)° \quad (5)$$

Fig. 13 shows a schematic diagram of the assumed failure surface. The previous method for calculating the uplift capacity of pile is presented in Eq. (6). Here, the shear force of the failure surface can be expressed through Eq. (7), and the weight of the soil within the failure surface can be expressed through Eq. (8).

$$\theta = 45° + \left(45 - \frac{\varphi_{sc}}{2}\right)° \quad (6)$$

$$\sum T_f = \left[\pi(b_{ct} + b_{cb})\sqrt{(b_{ct} - b_{cb})^2 + L_c^2}\right] \times \tau_{sc} \quad (7)$$

$$\sum W_s = \left[\frac{1}{3}\pi L_c(b_{ct}^2 + b_{ct}b_{cb} + b_{cb}^2)\right] \times \gamma_s \quad (8.1)$$

$$b_{ct} = \frac{L_c}{\tan(\theta_E)} + b_{ct} \quad (8.2)$$

$$L_c = L - \left(\frac{L1}{2} + L2\right) \quad (8.3)$$

$$b_{cb} = \frac{b_b}{2} - \left(\frac{\frac{b_b}{2}}{2} - b_s\right) / \tan(\theta_E) \quad (8.4)$$

After substituting Eqs. (7) and (8) into Eq. (6), new predictive model for the uplift capacity of belled pile in the soft-rock ground was proposed in Eq. (9).

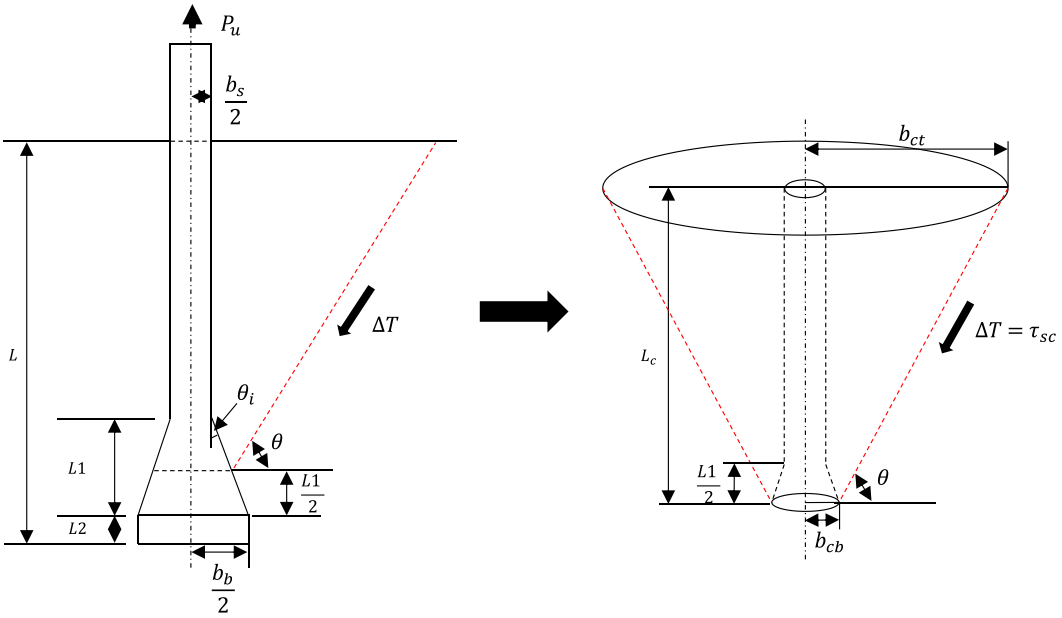

Fig. 13 Schematic diagram of the assumed failure surface

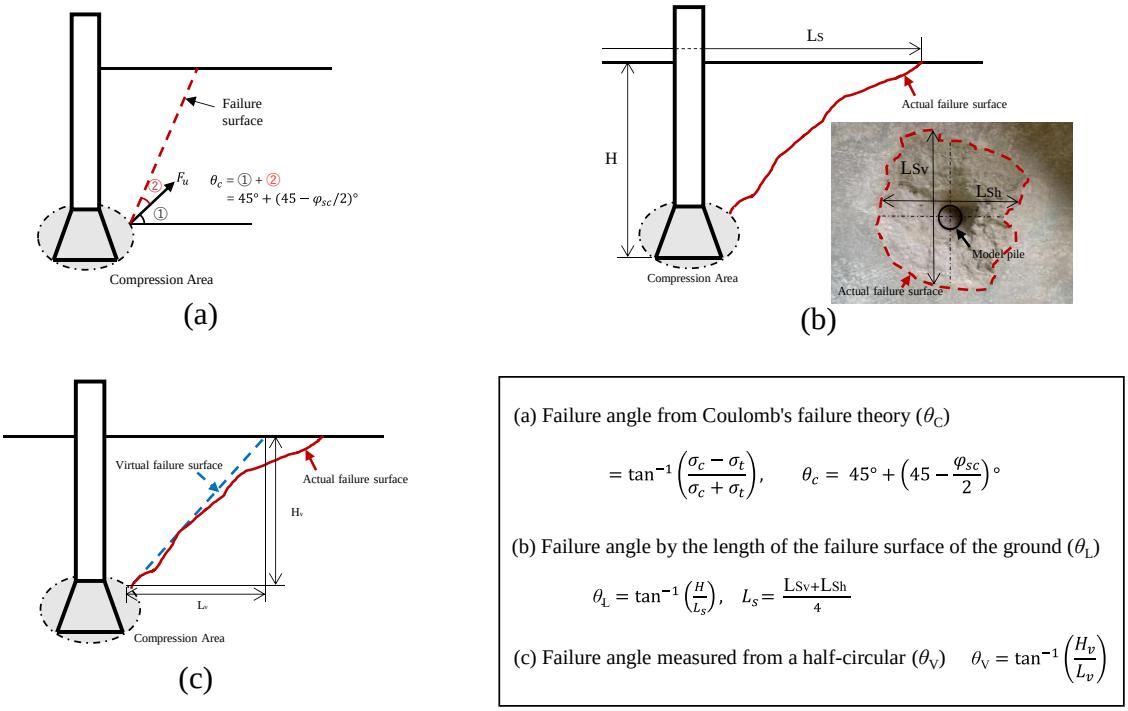

(a) Failure angle from Coulomb's failure theory (θ_C)

$$= \tan^{-1}\left(\frac{\sigma_c - \sigma_t}{\sigma_c + \sigma_t}\right), \quad \theta_c = 45° + \left(45 - \frac{\varphi_{sc}}{2}\right)°$$

(b) Failure angle by the length of the failure surface of the ground (θ_L)

$$\theta_L = \tan^{-1}\left(\frac{H}{L_s}\right), \quad L_s = \frac{LSv+LSh}{4}$$

(c) Failure angle measured from a half-circular (θ_V) $\quad \theta_V = \tan^{-1}\left(\frac{H_v}{L_v}\right)$

Fig. 14 Determination of failure surface according to different methods: (a) Coulomb's theory (θ_C), (b) Length of a failure surface (θ_L) and (c) Failure angle measured using image analysis

$$\therefore P_{u(net)} = \left\{\left[\frac{1}{3}\pi L_c(b_{ct}^2 + b_{ct}b_{cb} + b_{cb}^2)\right] \times \gamma_s\right\} + \left\{\left[\pi(b_{ct} + b_{cb})\sqrt{(b_{ct} - b_{cb})^2 + L_c^2}\right] \times \tau_{sc}\right\} \quad (9)$$

where W_{soil}: weight of the soil in the failure surface, W_{pile}: weight of the pile, T: shear stress at the failure surface, b_{ct}: diameter of the failure surface, b_{cb}: diameter of belled part, L_c: formation depth of failure surface from the surface, τ_{sc}: shear stress acting on the failure surface.

4.3 Validation of developed models

In this section, the calculated and experimental values were compared to verify the proposed predictive model for the uplift capacity in soft-rock ground. The main parameters in the proposed model are the failure angle, unit weight of the ground, and the shear force in the failure surface. Determining the failure angle is crucial in this model because of the difficulty of visually determining the failure angle in-situ. Therefore, the failure angle was verified from

Table 7 Determination of failure angle according to the three methods

Case ID	1) Coulomb's theory (θ_C)	2) Average length of a failure surface (θ_L)	3) Failure angle measured using image analysis (θ_V)
P00L16-1	60.0°	65.9°	-
P12L16-1	60.0°	33.1°	-
P12L08-1	60.0°	25.3°	-
HP12L88-1	60.0°	22.1°	63.3°
HP12L88-0.3	62.5°	33.3°	68.5°
HP30L88-1	60.0°	27.1°	65.8°

Table 8 Error rates of the three failure angle calculations and experimental values

Test ID	Experiment	1) Coulomb's theory (θ_C)		2) Length of a failure surface (θ_L)		3) Failure angle measured from a half-circular (θ_V)	
	(kN)	P_u (kN)	ε (%)	P_u (kN)	ε (%)	P_u (kN)	ε (%)
P12L16-1	9.03	7.74	16.7	15.25	97.0	-	-
P12L08-1	3.09	4.19	26.2	15.09	260.2	-	-
HP12L88-1	1.56	1.29	20.7	9.75	656.1	1.79	38.6
HP12L88-0.3	0.64	0.59	8.2	2.04	246.5	0.57	3.29
HP30L88-1	1.55	1.10	41.2	6.72	510.9	1.10	131.7

three failure angles obtained through observation of the failure surface in the laboratory model experiments (circular and half-circular chambers) and calculation by applying Coulomb's failure theory.

Three types of failure angle measurement methods were proposed in this study, as shown in Fig. 14. First, after fabricating a specimen under the same conditions as the model ground, the method of determining the failure angle through the internal friction angle from Coulomb's failure theory (Fig. 14(a)). The failure angle obtained from the circular model test was calculated by considering the average value of the horizontal and vertical lengths of the failure surface and the penetration depth (Fig. 14(b)). The failure angle from the half-circular model test was directly determined by measuring the slope of the actual failure surface from the observation window (Fig. 14(c)).

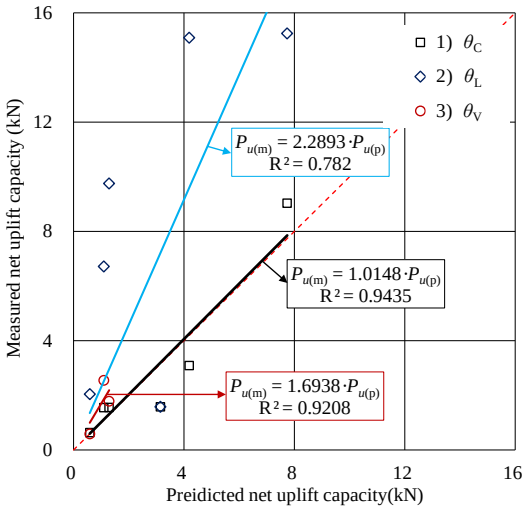

Fig. 15 Comparison of calculated and measured

Consequently, the failure angle was determined according to the measurement method as follows: 1) failure angle derived from Coulomb's theory (θ_C), 2) failure angle obtained from the average length of the failure surface of the ground surface from the circular chamber (θ_L), and 3) failure angle measured using the image analysis in the half-circular chamber (θ_V). Table 7 shows the results for each failure angle. The failure angles directly observed from the half-circular chamber were 63.3°~68.5°. The failure angle calculated from Coulomb's failure theory ranged from 60° to 62.5° according to the ground strength, and the results were similar to those of the directly observed failure angle. On the other hand, the failure angle calculated through the failure surface length of the ground surface in the circular model experiment differed by more than 45°.

Fig. 15 and Table 8 present the results for, and error rates between, the measured and predicted values using the three methods to determine the failure angle. To evaluate the accuracy of the predicted value, the predicted and experimental values under each condition were compared using the percentage error (PE), as presented in Eq. (10).

$$\therefore PE(\%) = \left|\frac{(U_{pm} - U_{pp})}{U_{pm}}\right| \cdot 100 \quad (10)$$

Where, U_{pm}: uplift capacity of the test value, U_{pp}: uplift capacity of the calculated value.

Accordingly, the failure angle measured in the half-circular chamber exhibited good agreement with the measured value. The PE of the calculated failure angle derived from Coulomb's failure theory ranged from 8.2 to 41.2%, which was closest to the measured value. In addition, The PE of the results obtained from the directly measured failure angle from the half-circular chamber ranged from 3.2 to 131.7%, corresponded to a relatively good prediction accuracy. On the other hand, the PE of the

failure angle calculated from the length of the failure surface at the ground surface was a maximum of 656.1%, indicating a predicted value higher than the measured value. Therefore, the results verified that Coulomb's failure theory and the derived failure angles measured from the half-circular chamber are useful for applying the proposed predictive model. In addition, the failure angle obtained from the length of the failure surface in the ground is not deemed suitable for applying the proposed predictive model. However, because it is impossible to determine the failure angle of the pile through in-situ field observations, the method of determining the failure theory obtained from Coulomb's failure theory is recommended for determining the failure angle of the proposed predictive model.

5. Conclusions

In this study, circular and half-circular model experiments and image analysis were performed to evaluate the uplift capacity characteristics and to failure mechanism of belled piles installed in soft-rock ground. The failure surface of soft-rock ground is affected by the ground strength, penetration depth, and the bell angle of the pile. In addition, a predictive model for the uplift capacity of a belled pile was proposed by considering the failure mechanism of a belled pile installed in soft-rock ground. The main conclusions drawn are as follows:

1. In the circular model test, the belled pile had higher uplift capacity than the conventional pile at the same penetration depth and ground strength. In addition, under the same belled pile and ground strength conditions, the uplift capacity at a penetration depth of 16 cm was 1.33 times higher than that at a penetration depth of 8 cm. In the half-circular model test, the difference in the uplift capacity according to the ground strength was marked. The difference in the uplift capacity according to the soil strength was confirmed to be approximately 1.9 times under the same penetration depth and belled pile angle. Additionally, the difference in the uplift capacity according to the belled angle was approximately 10%, and the influence of the belled angle was relatively low.
2. The shape of the failure surface in the half-circular model test was an inverted cone regardless of the uplift loading method, namely stress and strain control. In addition, the failure formation mechanism comprised three stages: (a) static, (b) compression, and (c) formation of the failure surface. In particular, the compression of the surrounding ground was a unique characteristic of soft-rock ground.
3. A new predictive model for the uplift capacity of a belled pile applicable to the soft-rock ground was proposed based on the previous predictive model. The main parameters in the proposed model were the failure angle, unit weight, and shear force within the failure surface. The starting point of the failure surface in the soft-rock ground under the model was assumed to be the center of the pile tip, and the characteristics of the failure surface formation of the ground, that is the inverted cone shape, were considered.
4. Determining the failure angle has a very important bearing on the parameters of this model because determining the failure angle in-situ in the field is difficult. Hence, determining the fracture angle involved three measurement methods as follows: 1) failure angle derived from Coulomb's theory (θ_C), 2) failure angle obtained from the average length of the failure surface of the ground surface from the circular chamber (θ_L), and 3) failure angle measured using the image analysis in the half-circular chamber (θ_V). The verification revealed that the predicted value was most similar to the experimental value of the directly observed failure angle, but observing the failure angle in the field is difficult. Hence, determining the failure angle through Coulomb's failure theory was recommended from the proposed model.

This study aimed to investigate the failure mechanism of soft-rock ground to propose a predictive model for the uplift capacity of the belled pile. However, no study on the failure mechanism of the belled pile installed in soft-rock ground has been conducted. Therefore, to validate the failure mechanism identified in this study in detail, further studies can be performed to examine the strengths of different soft-rock grounds, the uplift capacity for different belled angles, belled angle and shape characteristics, uplift loading condition, and loading rate.

Acknowledgments

This work was supported by the National Research Foundation of Korea (NRF) grant funded by the Korea government (MSIT) (No. 2021R1C1C2004070) and the research funds from Gwangju University in 2023.

References

Aksoy, H.S., Gör, M. and İnal, E. (2016), "A new design chart for estimating friction angle between soil and pile materials", *Geomech. Eng.*, **10**(3), 315-324. http://dx.doi.org/10.12989/gae.2016.10.3.315.

Ali, O.K. and Abbas, H.O. (2019), "Performance assessment of screw piles embedded in soft clay", *Civ. Eng. J.*, **5**, 1788-1798. http://dx.doi.org/10.28991/cej-2019-03091371.

Balla, A. (1961), "The resistance to breaking-out of mushroom foundations for pylons", *Proceedings of the 5th. Int. Conf. on SMFE*, **1**, 569-576.

Basha, A. and Azzam, W.R. (2018), "Uplift capacity of single pile embedded in partially submerged sand", *KSCE J. Civ. Eng.*, **22**, 4882-4890. https://link.springer.com/article/10.1007/s12205-017-1715-2.

Cerfontaine, B., Knappett, J.A., Brown, M.J. and Bradshaw, A.S. (2019), "Effect of soil deformability on the failure mechanism of shallow plate or screw anchors in sand", *Comput. Geotech.*, **109**, 34-45. https://doi.org/10.1016/j.compgeo.2019.01.007.

Chae, D., Cho, W. and Na, H.Y. (2012), "Uplift capacity of belled pile in weathered sandstones" *Int. J. Offshore Polar Eng.*, **22**(4), 297-305. https://onepetro.org/IJOPE/article-abstract/35536/Uplift-Capacity-of-Belled-Pile-In-Weathered.

Chaly, A., Hanna, A. and Hanna, M. (1991), "Uplift behavior of screw anchors in sand" *Asce J. Geotech. Eng.*, **117**(5).

Cheng, P., Guo, J., Yao, K. and Chen, X. (2022), "Numerical

investigation on pullout capacity of helical piles under combined loading in spatially random clay", *Mar. Georesour. Geotech.*, 1-14. https://doi.org/10.1080/1064119X.2022.2120843.

Das, B.M., Seeley, G.R. and Pfeifle, T.W. (1977). "Pullout resistance of rough rigid piles in granular soil", *Soils Found.*, **17**(3), 72-77. https://doi.org/10.3208/sandf1972.17.3_72.

Das, B.M. (1983), "A procedure for estimation of uplift capacity of rough piles", *Soils Found*., **23**(3), 122-126. https://doi.org/10.3208/sandf1972.23.3_122.

Dash, B.K. and Pise, P.J. (2003), "Effect of compressive load on uplift capacity of model piles", *J. Geotech. Geoenviron. Eng*., **129**(11), 987-992. https://doi.org/10.1061/(ASCE)1090-0241(2003)129:11(987).

Dickin, E.A. and Leung, C.F. (1990), "Performance of piles with enlarged bases subject to uplift forces", *Can. Geotech. J.*, **27**(5), 546-556. https://doi.org/10.1139/t90-070.

Downs, D.I. and Chieurzzi, R. (1966), "Transmission tower foundations", *J. Power Div.*, **92**(2), 91-114. https://doi.org/10.1061/JPWEAM.0000518.

Emirler, B., Tolun, M. and Laman, M. (2016), "Experimental investigation of the uplift capacity of group anchor plates embedded in sand", *Geomech. Eng.*, **11**(5), 691-711. http://dx.doi.org/10.12989/gae.2016.11.5.691.

Faizi, K., Armaghani, D.J., Sohaei, H., Rashid, A.S.A. and Nazir, R. (2015), "Deformation model of sand around short piles under pullout test", *Measurement*, **63**, 110-119. https://doi.org/10.1016/j.measurement.2014.11.028.

Hirai, Y., Wakai, S. and Aoki, M. (2016), "In-situ pull-out tests of cast-in-place concrete piles with belled enlargements", *Jpn. Geotech. Soc. Spec. Publ.*, **2**(41), 1478-1481. https://doi.org/10.3208/jgssp.JPN-012.

Honda, T. (2015), "Distinct element analysis on uplift resistance of belled and multi-belled piles in layered ground" *Proceedings of the TC105 ISSMGE Int. Symp. on Geomechanics from Micro to Macro*.

Hu, Z., Qu, S., Wang, Q., Guo, Y., Ji, Y. and Ma, J. (2023), "Pullout behaviour of belled piles under axial and oblique pull in soil-rock composite ground: An experimental study", *Int. J. Civ. Eng.*, **21**(4), 569-582. https://link.springer.com/article/10.1007/s40999-022-00778-1.

Ilamparuthi, K. and Dickin, E.A. (2001), "The influence of soil reinforcement on the uplift behaviour of belled piles embedded in sand", *Geotext. Geomembranes.*, **19**(1), 1-22. https://doi.org/10.1016/S0266-1144(00)00010-8.

Ilamparuthi, K. and Muthukrishnaiah, K. (1999), "Anchors in sand bed: delineation of rupture surface", *Ocean. Eng.*, **26**(12), 1249-1273. https://doi.org/10.1016/S0029-8018(98)00034-1.

Ilamparuthi, K., Dickin, E.A. and Muthukrisnaiah, K. (2002), "Experimental investigation of the uplift behaviour of circular plate anchors embedded in sand", *Can. Geotech. J.*, **39**(3), 648-664. https://doi.org/10.1139/t02-005.

JIS, R. (2009), 5210: Portland Cement. Japanese Stand. Assoc. Tokyo, Japan.

Johnson, S.M. and Kavanagh, C.T. (1968), The design of foundations for buildings, McGraw-Hill Book Company, New York, USA.

Kishida, H. (1963), "Stress distribution by model piles in sand", *Soils Found.*, **4**(1), 1-23. https://doi.org/10.3208/sandf1960.4.1.

Kranthikumar, A., Sawant, V.A., Kumar, P. and Shukla, S.K. (2017), "Numerical and experimental investigations of granular anchor piles in loose sandy soil subjected to uplift loading", *Int. J. Geomech.*, **17**(2), 4016059. https://doi.org/10.1061/(ASCE)GM.1943-5622.0000733.

Leshchinsky, D., Vahedifard, F. and Meehan, C.L. (2012), "Application of a hydraulic gradient technique for modeling the uplift behavior of piles in sand", *Geotech. Test. J.*, **35**(3), 400-408. 10.1520/GTJ103850.

Lin, J.G., Hsu, S.Y. and Lin, S.S. (2015), "The new method to evaluate the uplift capacity of belled piles in sandy soil", *J. Mar. Sci. Technol.*, **23**(4), 523-533. https://doi.org/10.6119/JMST-015-0511-2.

Lin, Y., Xiao, J., Le, C., Zhang, P., Chen, Q. and Ding, H. (2022), "Bearing characteristics of helical pile foundations for offshore wind turbines in sandy soil", *J. Mar. Sci. Eng.*, **10**(7), 889. https://doi.org/10.3390/jmse10070889.

Maeno, Y., Takatani, T., Takahashi, S. and Shimosako, K. (1997), "On Application of Pile with Expanding End to Offshore Structure", *Proceedings of the civil engineering in the ocean, Japan Society of Civil Engineers*, **13**, 399-404. https://doi.org/10.2208/prooe.13.399.

Majer, J. (1955), "Zur berechnung von zugfundamenten", *Osterr. Bauzeitschrift.*, **10**(5), 85-90.

Matsuo, M. (1967), "Study on the uplift resistance of footing (I)", *Soils Found.*, **7**(4), 1-37. https://doi.org/10.3208/sandf1960.7.4_1.

Matsuo, M. (1968), "Study on the uplift resistance of footing (II)", *Soils Found.*, **8**(1), 18-48. https://doi.org/10.3208/sandf1960.8.18.

Merifield, R.S. (2011), "Ultimate uplift capacity of multiplate helical type anchors in clay", *J. Geotech. Geoenviron. Eng.*, **137**(7), 704-716. https://doi.org/10.1061/(ASCE)GT.1943-5606.0000478.

Meyerhof, G.G. (1973), "Uplift resistance of inclined anchors and piles", *Proceedings of the 8th ICSMFE*, **2**, 167-172.

Meyerhof, G.G. and Adams, J.I. (1968), "The ultimate uplift capacity of foundations", *Can. Geotech. J.*, **5**(4), 225-244. https://doi.org/10.1139/t68-024.

Moayedi, H. and Mosallanezhad, M. (2017), "Uplift resistance of belled and multi-belled piles in loose sand", *Measurement*, **109**, 346-353. https://doi.org/10.1016/j.measurement.2017.06.001.

Mohajerani, A., Bosnjak, D. and Bromwich, D. (2016), "Analysis and design methods of screw piles: A review", *Soils Found.*, **56**(1), 115-128. https://doi.org/10.1016/j.sandf.2016.01.009.

Mosallanezhad, M. and Moayedi, H. (2017), "Developing hybrid artificial neural network model for predicting uplift resistance of screw piles", *Arab. J. Geosci.*, **10**(22), 479. https://link.springer.com/article/10.1007/s12517-017-3285-5.

Murray, E.J. and Geddes, J.D. (1987), "Uplift of anchor plates in sand", *J. Geotech. Eng.*, **113**(3), 202-215. https://doi.org/10.1061/(ASCE)0733-9410(1987)113:3(202).

Ovesen, N. K. (1981), "Centrifuge tests to determine the uplift capacity of anchor slabs in sand", *Proceedings of the 10th International Conference on Soil Mechanics and Foundation Engineering*, Stockholm, Sweden.

Perumalsamy, K. and Ranganathan, S. (2022), "Single pile in cohesionless soil in sloping ground under lateral loading", *Int. J. Geoeng*., **13**(1), 8. https://doi.org/10.1186/s40703-022-00173-8.

Prakash A.R. and Muthukkumaran, K. (2021), "Estimation of lateral capacity of rock socketed piles in layered soil rock profile", *Int. J. Geoeng*., **12**(11), 1-15. https://doi.org/10.1186/s40703-021-00140-9.

Qian, Z., Lu, X., Han, X. and Tong, R. (2015), "Interpretation of uplift load tests on belled piers in Gobi gravel", *Can. Geotech. J.*, **52**(7), 992-998. https://doi.org/10.1139/cgj-2014-0075.

Rao, S.N., Latha, K.H., Pallavi, B. and Surendran, S. (2006), "Studies on pullout capacity of anchors in marine clays for mooring systems", *Appl. Ocean Res.*, **28**(2), 103-111. https://doi.org/10.1016/j.apor.2006.08.001.

Robinsky, E.I. and Morrison, C.F. (1964), "Sand displacement and compaction around model friction piles", *Can. Geotech. J.*, **1**(2), 81-93. https://doi.org/10.1139/t64-002.

Roy, A., Chow, S.H., O'Loughlin, C.D. and Randolph, M.F. (2021), "Towards a simple and reliable method for calculating uplift capacity of plate anchors in sand", *Can. Geotech. J.*,

58(9), 1314-1333. https://doi.org/10.1139/cgj-2020-028.
Sakr, M., Nazir, A., Azzam, W. and Sallam, A. (2020), "Model study of single pile with wings under uplift loads", *Appl. Ocean Res.*, **100**, 102187. https://doi.org/10.1016/j.apor.2020.102187.
Santos Filho, J.M.D. and Tsuha, C.D.H.C. (2020), "Uplift performance of helical piles with cement injection in residual soils", *Can. Geotech. J.*, **57**(9), 1335-1355. https://doi.org/10.1139/cgj-2019-0317.
Sharif, Y.U., Brown, M.J., Cerfontaine, B., Davidson, C., Ciantia, M.O., Knappett, J.A., Ball, J.D., Brennan, A., Augarde, C. and Coombs, W. (2021), "Effects of screw pile installation on installation requirements and in-service performance using the discrete element method", *Can. Geotech. J.*, **58**(9), 1334-1350. https://doi.org/10.1139/cgj-2020-0241.
Spagnoli, G. and de Hollanda Cavalcanti Tsuha, C. (2020), "A review on the behavior of helical piles as a potential offshore foundation system", *Mar. Georesour. Geotechnol.*, **38**(9), 1013-1036. https://doi.org/10.1080/1064119X.2020.1729905.
Spagnoli, G., Gavin, K., Brangan, C. and Bauer, S. (2015), "In situ and laboratory tests in dense sand investigating the helix-to-shaft ratio of helical piles as a novel offshore foundation system", *Front. Offshore Geotech.*, **3**, 643-648.
Tsuha, C. de H.C., Aoki, N., Rault, G., Thorel, L. and Garnier, J. (2012), "Evaluation of the efficiencies of helical anchor plates in sand by centrifuge model tests", *Can. Geotech. J.*, **49**(9), 1102-1114. https://doi.org/10.1139/t2012-064.
Ukritchon, B. and Keawsawasvong, S. (2019), "Design equations of uplift capacity of circular piles in sands", *Appl. Ocean Res.*, **90**, 101844. https://doi.org/10.1016/j.apor.2019.06.001.
Vashishtha, H.R. and Sawant, V.A. (2021), "An experimental investigation for pullout response of a single granular pile anchor in clayey soil", *Int. J. Geoeng.*, **12**(35), 1-19. https://doi.org/10.1186/s40703-021-00162-3.
Vignesh, V. and Muthukumar, M. (2023), "Experimental and numerical study of group effect on the behavior of helical piles in soft clays under uplift and lateral loading", *Ocean Eng.*, **268**, 113500. https://doi.org/10.1016/j.oceaneng.2022.113500.
Wang, Q., Ma, J., Xiao, Z., Chen, W. and Ji, Y. (2020), "Field test on uplift bearing capacity of rock-socketed belled piles", *KSCE J. Civ. Eng.*, **24**(8), 2353-2363. https://doi.org/10.1007/s12205-020-2011-0.
Yamazaki, M. (1995), "Effect of underreamed end shapes on the structural strength of cast-in-place concrete pile ends", *J. Struct. Constr. Eng.*, **470**, 95-103.
Yang, B., Ma, J., Chen, W. and Yang, Y. (2018), "Uplift behavior of belled short piles in weathered sandstone", *Math. Probl. Eng.*, **2018**, 8614172. https://doi.org/10.1155/2018/8614172.

IC

Notation

b_b = Tip diameter of the belled pile
b_s = Shaft diameter of the belled pile
b_b = Tip diameter of the belled pile
b_{ct} = Diameter of the failure surface
b_{cb} = Diameter of belled part
θ = Failure angle
θ_C = Failure angle derived from Coulomb's theory
θ_L = Failure angle derived from surface failure length
θ_V = Failure angle determined from the image analysis
θ_t = Belled angle
H_v = Vertical length of the failure surface identified by image analysis
L = Pile penetration depth
L_v = Horizontal length of the failure surface identified by image analysis
L_c = Formation depth of failure surface from the surface
L_{Sv} = Maximum surface horizontal length of the failure surface
L_{Sv} = Maximum surface vertical length of the failure surface
P_u = Uplift capacity
$P_{u(Net)}$ = Net uplift capacity
T = Shear stress at the failure surface
U_{pm} = Uplift capacity of the test value
U_{pP} = Uplift capacity of the calculated value
τ_{sc} = Shear stress acting on the failure surface
σ_c = Compressive stress of specimen
σ_t = Tensile stress of specimen
W_{soil} = Weight of the soil in the failure surface
W_{pile} = Weight of the pile
φ_{sc} = Internal friction angle of specimen